Non-catalytic function of PRC2 in the control of small RNA dynamics during programmed genome elimination in *Paramecium*

Caridad Miró-Pina[1], Olivier Arnaiz[2], Augustin de Vanssay[1], Andrea Frapporti[1], Olivia Charmant[1], Adeline Humbert[1], Maoussi Lhuillier-Akakpo[1] and Sandra Duharcourt[1*]

[1] Université Paris Cité, CNRS, Institut Jacques Monod, F-75013 Paris, France.
[2] Université Paris-Saclay, CEA, CNRS, Institute for Integrative Biology of the Cell (I2BC), 91198, Gif-sur-Yvette cedex, France

Corresponding author: sandra.duharcourt@ijm.fr

Abstract

To limit transposable element (TE) mobilization, most eukaryotes have evolved small RNAs to silence TE activity via homology-dependent mechanisms. Small RNAs, 20-30 nucleotides in length, bind to PIWI proteins and guide them to nascent transcripts by sequence complementarity, triggering the recruitment of histone methyltransferase enzymes on chromatin to repress the transcriptional activity of TEs and other repeats. In the ciliate *Paramecium tetraurelia*, 25-nt scnRNAs corresponding to TEs recruit Polycomb Repressive Complex 2 (PRC2), and trigger their elimination during the formation of the somatic nucleus. Here, we sequenced sRNAs during the entire sexual cycle with unprecedented precision. Our data confirmed that scnRNAs are produced from the entire germline genome, from TEs and non-TE sequences, during meiosis. Non-TE scnRNAs are selectively degraded, which results in the specific selection of TE-scnRNAs. We provide important mechanistic insight into the scnRNA selection pathway by identifying PRC2 and its cofactors as essential for the selective degradation of non-TE-scnRNAs. Our findings reveal a new mechanism for PRC2 that involves a non-methyltransferase function for regulating small RNA dynamics during development.

Introduction

Small silencing RNAs bound to Argonaute/Piwi proteins target RNAs for degradation. Conversely, endogenous RNAs are able to trigger degradation of their cognate small RNA. Instances of target-directed degradation of microRNAs have been reported in mammalian cells, *Caenorhabditis elegans* and *Drosophila* (Han and Mendell, 2023). In ciliates, a different class of small RNAs, the scnRNAs, that resemble the metazoan Piwi-interacting RNAs (piRNAs), undergo selective degradation during developmentally programmed genome elimination (Lepere et al., 2009; Mochizuki et al., 2002; Sandoval et al., 2014; Schoeberl et al., 2012; Singh et al., 2014).

In the ciliate *Paramecium tetraurelia*, two types of nuclei coexist in the same cell: the germline micronucleus (MIC) and the somatic macronucleus (MAC). During the self-fertilization process of autogamy, the MIC undergoes meiosis and karyogamy to produce the zygotic nucleus. New MICs and new MACs develop from mitotic products of the zygotic nucleus (Figure 1A) (Betermier and Duharcourt, 2014). The MAC contains a reduced genome (72 Mb) compared to the MIC genome (108 Mb) as a result of massive and reproducible genome elimination (~30 Mb) that occurs at each sexual cycle (Aury et al., 2006; Guérin et al., 2017; Sellis et al., 2021). Eliminated sequences include 45,000 Internal Eliminated Sequences (IESs) that are remnants of transposable elements scattered throughout the genome (Sellis et al., 2021). Other Eliminated Sequences (OES) correspond to large regions comprising repeats such as transposable elements or satellites (Guérin et al., 2017).

The sites of DNA elimination do not seem to be specified by the DNA sequence in the MIC genome because, beyond an invariable TA at IES extremities, no strictly conserved sequence motif has been identified in or around IESs. Instead, DNA elimination is epigenetically controlled by the maternal MAC. For a subset of IESs, the artificial introduction of an IES in the maternal MAC was shown to inhibit the elimination of the zygotic IES in the new MAC of the sexual progeny (Duharcourt et al., 1998, 1995). To explain the sequence specificity of this maternal control, a model has been proposed whereby a crosstalk between the maternal MAC and the new MAC is achieved by a genome-wide sequence comparison mediated by RNA molecules (Mochizuki et al., 2002). 25-nt long scnRNAs produced from the germline MIC by the Dicer-like proteins Dcl2 and Dcl3 (Lepere et al., 2009; Sandoval et al., 2014; Singh et al., 2014) are bound to Ptiwi01/09 proteins and transported to the maternal MAC (Furrer et al., 2017). It is believed that scnRNAs are then sorted out by pairing interactions with nascent non-coding RNAs produced by the MAC genome (Figure 1A) (Aronica et al., 2008; Lepere et al., 2008; Mochizuki et al., 2002). Non-coding RNAs are thought to trigger the degradation of their cognate small RNA (MAC-scnRNAs), while scnRNAs corresponding to MIC-specific sequences (MIC-scnRNAs), which by definition cannot pair with MAC transcripts, are thought to be retained. This selective degradation of MAC-scnRNAs would thus result in the specific selection of the subpopulation corresponding to MIC-scnRNAs. In support of this model, the requirement of complementary MAC transcripts for scnRNA selection has been directly demonstrated in *Paramecium* (Lepere et al., 2008).

The complexes formed by MIC-scnRNAs bound to Ptiwi01/09 are transported from the maternal MAC to the new MAC. In a mechanism very similar to that described in fungi and metazoans (Martienssen and Moazed, 2015), scnRNAs target the Piwi proteins to complementary nascent transcripts (Maliszewska-Olejniczak et al., 2015) to guide heterochromatin formation in the new MAC, thereby providing specificity despite the lack of conserved motifs on eliminated sequences (Figure 1A). A physical interaction between Ptiwi09

and the Polycomb Repressive Complex 2 (PRC2-Ezl1) was recently shown to mediate the establishment of heterochromatin at scnRNA-targeted regions (Figure 1A) (Miró-Pina et al., 2022; Wang et al., 2022). PRC2-Ezl1 comprises a core complex and additional cofactors; the catalytic subunit Ezl1 trimethylates histone H3 on lysines 27 and 9 (H3K27me3 and H3K9me3) in the new MAC (Frapporti et al., 2019). Deposition of these repressive marks is essential for the elimination of transposable elements and of 70% of IESs (Frapporti et al., 2019; Lhuillier-Akakpo et al., 2014). Both H3K27me3 and H3K9me3 marks are associated with transposable elements (Frapporti et al., 2019). A second class of sRNAs called iesRNAs, produced from excised IES transcripts by a distinct Dicer protein, Dcl5, and bound to Ptiwi10/11, is reported to enhance the excision of a subset of IESs (Allen et al., 2017; Sandoval et al., 2014). Both classes of sRNAs appear to act synergistically in the new MAC. Indeed, RNAi-mediated co-depletion of the 3 Dicer proteins Dcl2, Dcl3 and Dcl5 inhibited the excision of 50% of IESs, while depletion of Dcl5 alone or co-depletion of Dcl2 and Dcl3 inhibited the excision of a much smaller subset of IESs (5 and 7% of IESs, respectively) (Lhuillier-Akakpo et al., 2014; Sandoval et al., 2014).

Although scnRNA selection is a key process in the regulation of DNA elimination, its molecular mechanism remains elusive. To further understand this mechanism, we sequenced small RNAs during the entire sexual cycle of autogamy with unprecedented precision. Our results provide a comprehensive picture of the dynamics of scnRNAs and of their timing of production. In addition, we uncover developmental-specific sRNA clusters which produce 23-nt long small interfering RNAs (siRNAs) in an RNA-dependent RNA polymerase 2 (RDR2)-dependent manner. We demonstrate that PRC2 and its cofactors are involved in scnRNA selection. We further show that selection occurs normally in a PRC2 catalytic mutant, unraveling a non-catalytic function of the methyltransferase PRC2 in the selective degradation of scnRNAs.

Results

Dynamics of small RNAs involved in genome elimination

To get a comprehensive picture of sRNA dynamics, we sequenced small RNA populations at 11 time points covering with unprecedented precision the entire sexual cycle of autogamy (self-fertilization) (Figure 1; Figure S1A for cytological description). The time course experiments covered the whole duration of pre- and post-zygotic nuclear events, including the time window during which DNA elimination occurs (Zangarelli et al., 2022). Small RNA populations were mapped with no mismatches against the reference genomes and subdivided in three categories according to their length: 23-nt for small interfering RNA (siRNAs); 25-nt for scnRNAs and 26-29 nt for iesRNAs (Figure 1B).

25-nt scnRNAs begin to accumulate as soon as meiotic cells are detected in the culture (t1) and persist until cells undergoing meiosis are no longer detected (T=10 hours) (Figure 1B and Figure S1A), in line with the idea that scnRNAs biogenesis occurs during the meiotic phase. We have observed that 100% of cells transformed with a high copy number of a GFP-*PTIWI09* transgene (Bouhouche et al., 2011) were arrested in early meiosis I, before each MIC yields four haploid nuclei (Figure S1B). In these cells, the GFP-Ptiwi09 fusion protein was localized in the maternal MAC and in the meiotic MICs (Figure S1B). Small RNA sequencing experiments showed that 25-nt scnRNAs accumulate in meiosis I-arrested cells (Figure S1C), indicating that scnRNAs are produced prior to or during early meiosis I.
As previously reported from the sequencing of small RNAs from three time points (early conjugation time point in (Singh et al., 2014), and early and late developmental stages during autogamy in (Sandoval et al., 2014)), our dataset of 11 time points during autogamy confirmed that scnRNAs are produced from both strands (Figure S1D) and covered the whole MIC genome (Figure 1C-D). This can be clearly observed when examining the mapping of 25-nt scnRNAs across an individual genomic region (Figure 1C), where MAC sequences, as well MIC sequences (IES or OES) are covered. Using the currently available draft genome assembly (Guérin et al., 2017), we found that >88 % of the MIC genome is covered by at least 1X of normalized sequencing depth, from the moment scnRNAs are detected (t1) and until T=5 hours (Figure 1D). No bias in scnRNA coverage between IESs and MAC-destined sequences could be observed at the early time points (until T=0 hours) (Table S1). We conclude that scnRNAs are produced from the whole MIC genome in *Paramecium tetraurelia*.
As autogamy proceeds, we observed an increase in the proportion of 25-nt scnRNAs mapping to OES or IES over scnRNAs mapping to MAC sequences (Figure 1B-C). This increase started from T=3 hours in our time course experiment, and by T=20 hours, scnRNAs mostly corresponded to MIC sequences (Figure 1B). As illustrated for an individual genomic region, scnRNAs cover the entire OES region, that comprises annotated transposable elements, and the IESs scattered in the flanking regions (Figure 1C). As reported for an early and a late developmental time points (Sandoval et al., 2014), the enrichment in MIC-scnRNAs is consistent with the predicted effect of scnRNA selection, whether it results from the degradation of MAC-scnRNAs or from the amplification of MIC-scnRNAs or a combination of both.

26-29-nt long iesRNAs accumulated at T=10 hours. They mostly mapped IESs (Figure 1B), and the highest iesRNA coverage is found at the extremities of IESs (Figure S2A), as previously

reported (Sandoval et al., 2014). We analyzed iesRNA coverage as a function of IES elimination timing (Figure S2A-B) (Zangarelli 2022). We found that iesRNA accumulation correlates with IES elimination timing and all IESs produce iesRNAs, whether they are excised early or late (Figure S2A-B). The biogenesis of iesRNAs has been shown to require the Dcl5 protein, while scnRNA production depends on the Dcl2 and Dcl3 proteins (Lepere et al., 2009; Sandoval et al., 2014). Very early excised IESs are not sensitive to Dcl5 depletion, even though they are covered by iesRNAs (Figure S2A). Therefore, we conclude that all IESs can produce iesRNAs, regardless of whether their excision depends on Dcl2/3, Dcl5, or both (Figure S2A). Similarly, scnRNAs are produced for all IESs (Figure 1D), although only a subset of IESs require Dcl2/3 for their excision (Lhuillier-Akakpo et al., 2014; Sandoval et al., 2014).

Identification of developmental-specific siRNA clusters

Studies have shown that siRNA pathways are active throughout the entire *Paramecium* life cycle (Bouhouche et al., 2011; Lepere et al., 2009; Marker et al., 2010). Although 23-nt siRNAs are present at low levels during most stages of the life cycle, their levels increase slightly during autogamy (Figure 1B). To investigate whether this increase is due to the production of siRNAs from specific genomic loci, we analyzed the sequencing data from all time points and mapped the 23-nt siRNAs on the MAC genome (see Methods). We identified 136 short-read clusters (SRCs) (Tables S2-S3) based on sequencing coverage (see Methods). As expected, 85/136 overlapped with previously described SRCs expressed constitutively during vegetative growth (Carradec et al., 2015; Karunanithi et al., 2019). We also discovered 29 development-specific SRCs, 16 of which had not been previously reported (Figure 2A; Figure S3A-C) and whose mean length is 451 nt (Figure S3A; Tables S2-S3). These 29 developmental-specific SRCs accumulated at T=5 hours and were still detected at T=45 hours (Figure 2A, Figure S3B-C). During this time frame, the developmental-specific SRCs accounted for the majority of 23-nt siRNAs (79% at T=10 hours mapped on the 29 developmental-specific SRCs) (Figure S3C). While scnRNAs are produced from both strands, siRNAs corresponding to these 29 SRCs were exclusively transcribed from one strand (Figure 2B). Because the 16 SRCs overlap with predicted genes, we examined the levels of messenger RNAs (Figure 2C). mRNA expression was detected at T=0 hours, earlier than that of SRCs, and with an apparent peak at T=5 hours and T=11 hours and low expression levels at T=45 hours. Overall, the mRNA expression profiles of SRCs appear not to correlate with the timing of siRNA expression emanating from SRCs. The fact that the predicted overlapping genes are smaller (median gene length 256 nt) than the average gene length (median gene length 1046 nt for all genes) raises the question of whether these RNAseq covered genes are lowly expressed coding genes or possibly pseudogenes. Moreover, for the 16 developmental-specific SRCs overlapping putative protein coding genes, we noted that sRNAs accumulated antisense to gene transcription for most of them (15/16) (Figure 2B), consistent with the idea that developmental-specific SRCs are not degradation products of gene messenger RNAs.

The *P. tetraurelia* genome has undergone several whole genome duplications (WGDs) in the course of evolution, the last one dated before the radiation of the *aurelia* species complex (Aury et al., 2006; Sellis et al., 2021). We retrieved the paralogous region stemming from the last WGD for each developmental-specific SRC (Figure 2D, Figure S3D). We identified paralogous SRCs for some of them (6/29) which indicate that those correspond to conserved SRCs. In contrast, in the other cases, the paralogous regions were either lost or no SRC could

be detected (23/29), indicating that these SRCs may have been either acquired more recently, after the last WGD, or lost on the paralogous region.
To identify factors involved in the biogenesis of developmental-specific SRCs, we focused on two RNA-dependent RNA polymerases (Rdr1 and Rdr2) known to control the accumulation of endogenous siRNAs. Rdr2 was previously shown to be involved in the production of endogenous siRNAs (Marker et al., 2014) and a strong reduction in the accumulation of siRNAs from a few constitutive SRCs was reported with the rdr2-1.24 allele (Carradec et al., 2015) (Figure 2E). A null mutant of *RDR1* (rdr1-5.28 allele) also impaired accumulation of endogenous siRNAs (Carradec et al., 2015; Karunanithi et al., 2019) (Figure 2E). We sequenced the small RNA populations in these two rdr1 and rdr2 mutants at three time points (T=0; T=10 and T=20 hours) during an autogamy time course experiment. While the rdr1 mutant had no impact on the accumulation of developmental-specific SRCs, accumulation of siRNAs from the developmental-specific SRCs was completely abolished in the rdr2 mutant (Figures 2D-E, Figure S3B-S3D). In conclusion, we identified a novel class of endogenous developmental-specific clusters producing 23-nt long sRNAs, which map the MAC genome, are antisense to predicted transcription gene units, and are strictly dependent on Rdr2.

PRC2-Ezl1 core complex and its associated cofactors are involved in scnRNA selection

ScnRNA selection is thought to occur in the maternal MAC during MIC meiosis (Figure 1A). Proteins involved in this process would thus be localized in the maternal MAC at this time of the sexual cycle. While the PRC2-Ezl1 complex catalyzes deposition of H3K27me3 and H3K9me3 in the new MAC, it is first localized in the maternal MAC where it catalyzes solely H3K27me3 (Frapporti et al., 2019; Lhuillier-Akakpo et al., 2014; Miró-Pina et al., 2022). To assess whether PRC2-Ezl1 is involved in the selection process, we sequenced small RNA populations during autogamy at three different time points (T=0; T=10 and T=35 hours) in cells depleted for the PRC2-Ezl1 core components Ezl1 and Suz12.like and for the accessory proteins Rf2, Eap1 and Rf4 (Figure 3A and S3B-S4A-B). As previously described upon depletion of PRC2-Ezl1 components 7/4/23 5:26:00 PM, the 25-nt scnRNAs are produced from the MIC genome at the beginning of the sexual cycle (T=0 hours) with the same proportions of MAC, OES and IES scnRNAs as in control RNAi conditions. In contrast, depletion of the scnRNA biogenesis factors Dcl2/3 leads to the loss of scnRNAs (Figure 3A) (Furrer et al., 2017; Sandoval et al., 2014). However, as development proceeds (T=10 and T=35 hours), MIC-specific scnRNAs (OES + IES) are not enriched over MAC-specific scnRNAs in PRC2-Ezl1-depleted cells, indicating an absence of MIC-specific scnRNA selection (Figure 3A-B and S4A). Importantly, because we still detect maternal MAC ncRNA production in the *EZL1* knockdown experiments, the lack of scnRNA selection cannot be explained by a lack of maternal MAC ncRNA transcription (Figure S4C). A defect in scnRNA selection was also reported in cells depleted for the PRC2 core subunit Caf1 (Ignarski et al., 2014). Therefore, scnRNA selection relies on an intact PRC2 core complex, involving Ezl1 and its protein partners. In contrast, we noted that depletion of PRC2-Ezl1 core components and associated cofactors had no apparent impact on the accumulation of 23-nt developmental-specific SRCs (Figure S3B).
To determine whether impairment of scnRNA selection could be explained by defects in the localization of scnRNAs, we analyzed the localization of the scnRNA-binding protein Ptiwi09 with a *GFP-PTIWI09* transgene. In control cells, the fusion protein GFP-Ptiwi09 was detected in the cytoplasm and in the maternal MAC during MIC meiosis then localized exclusively in the developing MAC (Figure 3C). In contrast, in Dcl2/3-depleted cells, in which scnRNA biogenesis

is abrogated, the fusion protein GFP-Ptiwi09 was no longer detected during MIC meiosis and MAC development (Figure 3C). This observation is consistent with unloaded Argonaute proteins being generally unstable (Martinez and Gregory, 2013; Smibert et al., 2013). Thus, GFP-Ptiwi09 localization likely reflects scnRNA localization. In Ezl1-depleted cells, where scnRNA selection is defective, GFP-Ptiwi09 still localized in the maternal MAC during MIC meiosis then in the new developing MACs, as in control conditions (Figure 3C). In conclusion, the lack of MIC-specific scnRNA selection in the absence of Ezl1 does not appear to be associated with the mis-localization of scnRNAs.

scnRNA selection occurs in the absence of H3K27me3 in the maternal MAC

PRC2-Ezl1 catalyzes H3K27me3 in the maternal MAC (Frapporti et al., 2019; Lhuillier-Akakpo et al., 2014). To directly assess whether H3K27me3 is required for scnRNA selection, we sought to identify an experimental condition where H3K27me3 no longer accumulates in the maternal MAC. We designed a mutant H3 transgene carrying a lysine to methionine substitution in position 27 (H3K27M), a mutation described to cause a dominant negative effect preventing H3K27me3 accumulation at the endogenous H3 by inhibiting the enzymatic activity of PRC2 and resulting in genome-wide depletion of H3K27me3 (Bender et al., 2013; Lewis et al., 2013).
Five H3 proteins are encoded in the *Paramecium tetraurelia* MAC genome. H3P1 and H3P3 are H3.1 histones and are constitutively expressed during the life cycle (Lhuillier-Akakpo et al., 2016). *Paramecium* cells were transformed with histone *H3P1* or *H3P3* transgenes bearing K27M mutations and sexual events were triggered. Transformation with *H3P1*^{K27M} or *H3P3*^{K27M} transgenes abolished H3K27me3 deposition in the maternal MAC without affecting H3K27me3 deposition in the new developing MACs based on immunofluorescence experiments (Figure 4A). This does not appear to be due to a mislocalization of Ezl1 because in cells co-transformed with *H3P3*^{K27M} and *FLAG-EZL1* transgenes, the fusion protein Flag-Ezl1 correctly localized in the MIC and the maternal MAC during meiosis I then in the developing MACs (Figure S5A) (Lhuillier-Akakpo et al., 2014). Testing elimination of some IESs did not reveal any DNA elimination defect (Figure S5B) and the survival of the sexual progeny was not affected (Figure 4B), indicating that deposition of H3K27me3 in the maternal MAC did not appear to be required for IES elimination and viability of the sexual progeny. We sequenced the small RNA populations at two time points in *H3P1*^{K27M} transformed cells (Figure S5C-D). The scnRNAs were produced normally at early developmental stages (T=0 hours) and were enriched in MIC-specific sequences at later stages (T=20 hours) (Figure 4C and S5C-D). Thus, the scnRNA selection process does not appear to require H3K27 trimethylation in the maternal MAC. Consistent with this observation, H3K27me3 deposition is not affected in the maternal MAC of Eap1-depleted cells (Miró-Pina et al., 2022), while scnRNA selection is impaired (Figure 3).

Ezl1 catalytic activity is not required for scnRNA selection

Our data indicated that PRC2-Ezl1, but not its signature H3K27me3 in the maternal MAC, is necessary for scnRNA selection. We hypothesized that PRC2-Ezl1 functions in scnRNA selection was to methylate other substrates than K27 of H3. To test this possibility, we used a catalytic mutant of Ezl1. The H526A mutation in the SET domain of Ezl1 was previously shown to abolish Ezl1 catalytic activity *in vitro* and *in vivo* (Frapporti et al., 2019). H3K27me3 no longer

accumulated in the maternal MAC nor in the new developing MACs in the mutant, even though the mutant Ezl1 protein still correctly localized (Figure 4D). In cells expressing the RNAi-resistant *GFP-EZL1*^{H526A} mutant transgene and silenced for the endogenous *EZL1* gene, we performed *s*mall RNA sequencing. Contrary to our expectations, scnRNAs were produced normally at the beginning of the sexual cycle (T=0 hours) and MIC-specific scnRNAs were correctly selected at later stages (T=35 hours) (Figure 4C and S5C-D). Thus, we conclude that the function of PRC2-Ezl1 in scnRNA selection is independent of its methyltransferase activity.

Discussion

This study provides a comprehensive description of small RNA populations during the sexual process of autogamy in *Paramecium tetraurelia*. We uncovered the existence of developmental-specific 23-nt siRNA clusters, which are in antisense orientation to the transcription of putative coding genes they overlap with. We showed that accumulation of siRNAs from the developmental-specific SRCs is controlled by the RNA-dependent RNA polymerase Rdr2 but not Rdr1. While Rdr1 plays a role in the dsRNA-induced RNAi pathway, Rdr2 was previously shown to be required for all known types of siRNAs in *Paramecium*, including endogenous siRNAs from constitutive SRCs (Carradec et al., 2015; Karunanithi et al., 2019). A separate study reported that developmental-specific SRCs are bound to the Ptiwi08 protein and appear to be Dicer 1-dependent (Solberg et al., 2023). The biological roles of the 23-nt siRNAs produced from the developmental-specific SRCs and of Rdr2 remain unclear. Further analyses will be needed to determine whether, as hypothesized in Solberg et al., 2023, developmental-specific SRCs regulate aberrant, untranslated mRNAs during development, or instead play a role in other processes such as gene copy number control during development, or act as an antiviral defense mechanism.

Using cells arrested in meiosis I, we demonstrated that scnRNAs accumulated prior to or during early meiosis I. Covering the entire sexual cycle of autogamy with sRNA sequencing at 11 time points, we determined, at an unprecedented resolution, that scnRNAs are produced from both strands for the whole MIC genome in *Paramecium tetraurelia*, with no bias in scnRNA coverage between IESs and MAC-destined sequences. The mechanism underlying this genome-wide transcription is studied but remains elusive (Gruchota et al., 2017; Owsian et al., 2022).
After scnRNAs are produced from the entire MIC genome, genome-wide degradation of MAC-scnRNAs occurs; the earliest time at which degradation is detected corresponds to the onset of DNA elimination. As a result of this specific degradation, the subpopulation of scnRNAs corresponding to MIC-specific sequences is selected and persists until the end of MAC development. The dynamics of scnRNAs we observed during *Paramecium* sexual events contrasts with that described in another ciliate, *Tetrahymena thermophila* (Schoeberl et al., 2012). Indeed, during *Tetrahymena* conjugation, scnRNAs are preferentially produced from eliminated sequences, resulting in a biased production of scnRNAs from MIC-specific sequences. In addition, there is a rather limited selection process. The massive degradation of MAC-scnRNAs (> 70 Mb of complexity) makes *Paramecium* a very good model to decipher the mechanisms involved.

Here, we showed that RNAi-mediated knockdown of genes encoding core components of the PRC2-Ezl1 core complex (Ezl1 and Suz12.like) and its associated cofactors (Rf2, Rf4 and Eap1)

prevented scnRNA selection. Thus, the PRC2-Ezl1 complex is involved in MAC-scnRNA degradation, in agreement with previous studies (Ignarski et al., 2014; Wang et al., 2022). In cells depleted for Ezl1, Suz12.like and Rf2, the PRC2-Ezl1 complex collapses, while in the absence of the accessory factor Rf4, the physical association between PRC2-Ezl1 and Ptiwi09 is abrogated in the new MAC (Miró-Pina et al., 2022). Eap1 depletion does not alter the interaction between the PRC2-Ezl1 components nor the interaction of the complex with Ptiwi09 (Miró-Pina et al., 2022). Ezl1 has been shown to transiently localize in the maternal MAC, where the selection process likely occurs, before it is detected in the new developing MACs (Lhuillier-Akakpo et al., 2014). Likewise, Ezl1-interacting partners are also transiently localized in the maternal MAC before they localize in the new MAC (Miró-Pina et al., 2022). If the composition of the complex is similar in the maternal MAC and in the new MAC, we conclude that PRC2-Ezl1 function in scnRNA selection requires the integrity of the complex, its interaction with Ptiwi09, and the accessory factor Eap1, whose exact role remains to be determined.
Monitoring the localization of the scnRNA-binding protein Ptiwi09 indicated that the scnRNA-Ptiwi09 complexes are correctly localized, despite the lack of selection in PRC2-Ezl1 depleted cells. Thus, in absence of selection, both MAC- and MIC- scnRNAs are present in the new MAC, a situation that is radically different from wild-type cells, where only MIC-scnRNAs are present in the new MAC and guide heterochromatin formation at target DNA sequences (Miró-Pina et al., 2022). We conclude that the mere presence of scnRNA-Ptiwi09 complexes in the new MAC does not appear to be sufficient to trigger DNA elimination, confirming that the PRC2-Ezl1 components are important for DNA elimination to occur (Miró-Pina et al., 2022).

We showed that the specific abrogation of H3K27me3 in the maternal MAC, the signature of PRC2-Ezl1, had no impact on scnRNA selection, demonstrating that this mark does not play a role in this process. To suppress H3K27me3, we expressed dominant negative forms of the H3.1 protein in which lysine 27 is replaced by a methionine ($H3P1^{K27M}$ and $H3P3^{K27M}$) (Bender et al., 2013; Lewis et al., 2013). These mutant proteins prevented the accumulation of H3K27me3 in the maternal MAC, but not in the new MAC, even though the mutated H3 and the PRC2 catalytic subunit Ezl1 were detected in both nuclei. The reason why the dominant negative effect of the H3.1 mutant protein is restricted to the maternal MAC is not known. The molecular mechanism by which H3K27M reduces H3K27me2/3 in cells remains a matter of debate more generally (Jain et al., 2020; Sarthy et al., 2020). Post-translational modifications of the same H3 tail, both proximal and distal to K27M, can greatly diminish the inhibition of PRC2 (Brown et al., 2014). Furthermore, the H3K27M-to-PRC2 stoichiometric ratio is believed to dictate the degree of PRC2 inhibition (Stafford et al., 2018). Thus, we speculate that H3.1 mutant proteins are unable to exert a dominant negative effect in the developing MACs because (i) H3P1 and H3P3 are not the substrates of PRC2-Ezl1 in the developing MACs; (ii) H3P1 and H3P3 in the developing MACs bear post-translational modifications that impede the dominant negative effect of the H3K27M mutation; or (iii) the amounts of PRC2 relative to H3K27M in the developing MACs are too high to be sensitive to H3K27M-mediated inhibition of PRC2 activity.
We did not observe any apparent consequence of the lack of H3K27me3 in the maternal MAC on DNA elimination and sexual progeny production. Therefore, we conclude that H3K27me3 deposition in the maternal MAC is not required for DNA elimination or sexual progeny production. At this point, the role of H3K27me3 in the maternal MAC remains elusive. If

H3K27me3 controls gene expression, it might not involve the expression of genes necessary for sexual events.

Our findings prompted us to investigate whether PRC2-Ezl1 might function through a different mechanism, independent of H3K27 methylation. Like many histone-modifying enzymes, the mammalian PRC2 has non-histone substrates, including the nuclear receptor Retinoid-Related Orphan Receptor Alpha (Lee et al., 2012), the transcription factor GATA4 (He et al., 2012), the facultative PRC2 cofactors JARID2 (Sanulli et al., 2015) and PAL1 (Zhang et al., 2021), and the RNAPII transcription elongation factor Elongin A (Ardehali et al., 2017). To assess whether PRC2-Ezl1 function in the scnRNA selection process may be decoupled from its methyltransferase activity, we tested a catalytic dead mutant of Ezl1, carrying a histidine-to-alanine substitution in its catalytic SET domain (H526A) (Frapporti et al., 2019). We showed that scnRNA selection occurred normally in the *EZL1*^{H526A} catalytic mutant, demonstrating that PRC2-Ezl1 has a function independent of its methyltransferase activity. One example of a non-catalytic function of the mammalian PRC2-Ezh1 was previously shown in an experimental setup where the artificial recruitment of a catalytically inactive Ezh1 led to transcriptional repression of a reporter via chromatin compaction (Margueron et al., 2008). The exact mechanisms by which PRC2-Ezl1 exerts its function in the scnRNA selection process independently of its methyltransferase activity remains an open question.
The scanning model proposes that the discrimination between MAC- and MIC-scnRNA/Ptiwi09 complexes results from the pairing of scnRNAs with complementary nascent non-coding transcripts produced by the maternal MAC. Only MAC-scnRNAs are degraded. One potential mechanism involves the post-transcriptional modification 2'-O-methylation at the 3' terminus by the methyl transferase HEN1. *Tetrahymena* scnRNAs, like piRNAs in metazoans, are 2'-O-methylated at their 3' ends (Ji and Chen, 2012; Kurth and Mochizuki, 2009). Hen1p-mediated 2'-O-methylation was reported to stabilize scnRNAs. Loss of Hen1p causes a reduction in the abundance and length of scnRNAs, defects in programmed genome elimination, and low production of sexual progeny (Kurth and Mochizuki, 2009). One could imagine that the scanning process leads to the differential 2'-O-methylation of MAC- and MIC-scnRNAs: MIC-scnRNAs would be 2'-O-methylated, which would protect them from degradation, while MAC-scanRNA would not. Data from a recent study contradicts this hypothesis, because *HEN1* KD during *Paramecium* autogamy did not impair scnRNA selection (Solberg et al., 2023). Thus, 2'-O-methylation of scnRNAs does not appear to be involved in the selection process.
Only MAC-scnRNAs display extensive complementarity with the non-coding RNA targets. We propose that the pairing between MAC-scnRNAs and MAC non-coding RNA leads to the degradation of the Ptiwi09 protein and its bound scnRNAs. In essence, the proposed mechanism is similar to microRNA target-directed degradation, in which pairing of the miRNA to the cognate RNA recruits a Cullin-RING E3 ubiquitin-ligase complex, leading to ubiquitination and proteasomal degradation of Ago and of the miRNA (Han et al., 2020; Shi et al., 2020). Based on our findings, we propose that a non-catalytic function of PRC2-Ezl1 in the degradation of MAC-scnRNAs contributes to the stabilization of the interaction between MAC-scnRNA/Ptiwi09 complexes and nascent non-coding RNAs, perhaps through an architectural role of PRC2-Ezl1 (Figure 4E). Alternatively, the non-catalytic function of PRC2 might be mediated by its cofactors, such as Eap1, which is involved in scnRNA selection and yet is not necessary for the stability of the PRC2-Ezl1 complex nor for its interaction with Ptiwi09. Future

work will be needed to elucidate the mechanisms at play and whether they are analogous to those involved in microRNA target-directed degradation.

MATERIALS AND METHODS

Paramecium strains, cultivation, and autogamy

Experiments were carried out with the entirely homozygous strain 51 of *P. tetraurelia* (wild-type or mutants nd7-1). We used two Rdr mutant strains isolated in (Marker et al., 2014). The rdr1-5.28 line corresponds to a putative null allele for Rdr1, containing a frameshift mutation leading to a premature stop codon upstream of the catalytic domain. The rdr2–1.24 line is a strong hypomorphic allele that retains an intragenic IES (located downstream of the conserved RdRP domain region), due to a T-to-A mutation in one of the boundaries required for excision during macronuclear development. Cells were grown in wheat grass powder (WGP) infusion medium bacterized the day before use with *Klebsiella pneumoniae*, unless otherwise stated, and supplemented with 0.8 mg/mL β-sitosterol. Cultivation and autogamy were carried out at 27 °C as described (Beisson et al., 2010a, 2010b).

Gene silencing experiments

For T7Pol-driven dsRNA production in silencing experiments plasmids L4440 with fragments of each gene and *Escherichia coli* strain HT115 DE3 were used. Sequences used for silencing of *ICL7a, EZL1, SUZ12.like*, *RF2*, *RF4*, *EAP1*, *DCL2* and *DCL3* were segments 1-580 of PTET.51.1.G0700039 (*ICL7a*); 989-1501 of PTET.51.1.G1740049 (*EZL1*); 590-946 of PTET.51.1.G0190277 (*SUZ12.like*); 1514-1916 of PTET.51.1.G1190062 (*RF2*); 623-1038 of PTET.51.1.G0570234 (*RF4*); 298-486 of PTET.51.1.G1310069 (*EAP1*); 434-1032 of PTET.51.1.G0210241 (*DCL2*) and 630-1468 of PTET.51.1.G0990073 (*DCL3*) as previously published (Garnier et al., 2004; Lepère et al., 2009; Lhuillier-Akakpo et al., 2014; Miró-Pina et al., 2022). Preparation of silencing medium and RNAi during autogamy were performed as described in (Baudry et al., 2009).

Transformation with tagged fusion transgenes

The *GFP-PTIWI09*, *GFP-EZL1*^{H526A} and *3XFLAG-HA-EZL1* were previously described (Bouhouche et al., 2011; Frapporti et al., 2019). For the construction of *H3*^{K27M} mutant transgenes, the lysine-coding triplet AAA from nucleotide 85 to 87 (K27) was replaced by ATG (methionine) by inverse PCR. Each gene was expressed under the control of their transcription signals (promoter and 3'UTR). The *H3P1* (PTET.51.1.G1450006) transcription signals contains 150-bp upstream and 192-bp downstream of its open reading frame. The *H3P3* (PTET.51.1.G0270094) transcription signals contains 89-bp upstream and 147-bp downstream of its open reading frame. For the *H3P3*^{K27M}*-GFP* construct, a GFP tag codon-optimized for the *P. tetraurelia* genetic code was added by RF cloning to the 3' end of the gene. Plasmids carrying the transgenes were linearized with restriction enzymes and microinjected into the MAC of vegetative 51 cells in the macronucleus.

Survival tests

Lethality of post-autogamous cells was assessed by transferring 30–60 individual post-autogamous cells to standard growth medium. Cells with a functional new MAC were identified as normally growing survivors unable to undergo a novel round of autogamy if starved after ~8 divisions.

Indirect immunofluorescence

Cells were fixed as previously described (Frapporti et al., 2019). For immunofluorescence, fixed cells were incubated overnight at room temperature with primary antibodies as follows: rabbit anti-H3K9me3 (1:200), rabbit anti-H3K27me3 (1:1000) (Frapporti et al., 2019) and mouse anti-FLAG (1:200) (Thermo Fisher Scientific Cat#MA1-91878; RRID: AB_1957945). Cells were labeled with Alexa Fluor 568-conjugated goat anti-rabbit IgG (Thermo Fisher Scientific Cat#A-11036; RRID: AB_10563566) or Alexa Fluor 568-conjugated goat anti-mouse IgG (Thermo Fisher Scientific Cat#A-11031; RRID: AB_144696) at 1:500 for 1 h, stained with 1 µg/mL Hoechst for 5–10 min and finally mounted in

Citifluor AF2 glycerol solution (Biovalley Cat#AF2-25). Images were acquired using a Zeiss LSM 780 or 710 laser-scanning confocal microscope and a Plan-Apochromat 63 × /1.40 oil DIC M27 objective. Z-series were performed with Z-steps of 0.35 µm.

DNA extraction and PCR

DNA samples were prepared from ≤1,000 autogamous cells using the NucleoSpin Tissue kit (Macherey-Nagel). For PCR analysis of IES excision, PCR amplifications were performed with Expand Long Template Enzyme mix (Expand Long Template PCR system, Roche). Oligos are available in Table S4.

RNA extraction, RT-PCR and sequencing

RNA samples were extracted from 200–400-mL cultures at 2,000–4,000 cells/mL as previously described (Frapporti et al., 2019) at different time points during autogamy. For RT-PCR, RNA samples were reverse-transcribed with RevertAid H Minus Reverse Transcriptase (Thermo Scientific) using polydT primers (Thermo Scientific) according to the manufacturer's instructions. It was then followed by PCR amplifications in a final volume of 25 µL, with 10 pmol of each primer, 10 nmol of each dNTP and 2 U of DyNAzyme II DNA polymerase (Thermo Scientific). For sRNA-seq, small RNAs of 15-30 nt were purified from total RNA on a 15% TBU/Urea gel. Small RNA libraries were constructed using the NEBNext Small RNA kit according to the manufacturer recommendations. The quality of the final libraries was assessed with an Agilent Bioanalyzer, using an Agilent High Sensitivity DNA Kit. Libraries were pooled in equimolar proportions and sequenced using a single read 75 pb run on an Illumina NextSeq500 instrument, using NextSeq 500 High Output 75 cycles kit.

Bioinformatic analyses

Sequencing data were demultiplexed using CASAVA (v1.8.2) and bcl2fastq2 (v2.18.12). Illumina adapters were removed using cutadapt (v1.12), keeping only reads with a minimal length of ten nucleotides. Paired-end reads were mapped on expected contaminants (mitochondrial genomes, ribosomal DNA, and bacterial genomes). sRNA-seq data were mapped on reference genomes using BWA (v0.7.15 -n 0). Only uniquely mapping reads were considered. sRNA-seq data were analyzed as previously (de Vanssay et al., 2020). Sequencing metrics are available in Table S5.

Reference genomes, software and R packages

Sequencing reads were mapped on expected contaminants (mitochondrial genomes, ribosomal DNA, and bacterial genomes) then mapped on *Paramecium* genome references using BWA (v0.7.15) and without any mismatches. The *P. tetraurelia* strain 51 reference genomes used in this study were : the MAC (ptetraurelia_mac_51.fa), the MAC+IES (ptetraurelia_mac_51_with_ies.fa) and the MIC (ptetraurelia_mic2.fa) (Arnaiz et al., 2012; Guérin et al., 2017). Gene annotation v2.0 (ptetraurelia_mac_51_annotation_v2.0.gff3), IES annotation v1 (internal_eliminated_sequence_PGM_ParTIES.pt_51.gff3) were also used (Arnaiz et al. 2020, Arnaiz et al. 2012)(Arnaiz et al., 2020, 2012). All files are available from the ParameciumDB download section (https://paramecium.i2bc.paris-saclay.fr/download/Paramecium/tetraurelia/51/) (Arnaiz et al., 2020). R (v4.0.4) packages were used to generate images (ggplot2 v3.3.5; ComplexHeatmap v2.6.2; GenomicRanges v1.42 ; rtracklayer v1.50).

sRNA quantification

The 20–30 nt sRNA reads were successively mapped on the MAC, MAC+IES and MIC genomes to attribute them to a specific genome compartment: MAC-destined sequence (MDS), Internal Eliminated Sequences (IES) or Other Eliminated Sequences (OES). In the case of a silencing experiment, the 23nt siRNA reads that map to the RNAi targets were removed. Read counts were normalized using the number sequenced reads using a G+C content < 50%, compatible with a *Paramecium* G+C genomic content (~27%).

Genome coverage of scnRNAs

To analyse the evolution of sRNA genome coverage, the sequencing data were sampled to 15M reads between 20 and 30 nt long. After mapping on the MIC genome, only 25-nt sRNA were kept. The coverage of the MIC genome was calculated using bamCoverage (deeptools v2.0) and a bin window of 100 nt. Using this window coverage, the percentage of genome covered by at least 1X was determined for each sample.

sRNA clusters

Only sRNAs of 23-nt in length mapped on the MAC genome were considered. Sequencing data from all the wild-type autogamy time course were merged to stringently annotate 136 short read clusters (SRC) using the program ShortStack (v3.8.5 --nohp --mincov 1000 --pad 100) (Johnson et al., 2016). The boundaries of these SRCs were manually adjusted and compared to, already published, vegetative SRCs with a minimum overlap of 23-nt (Carradec et al., 2015; Karunanithi et al., 2019) (see Table S3). The number of 23-nt sRNAs were counted on each SRC, with the information regarding transcription orientation, and normalized by the total number of sequenced sRNAs (20-30 nt with GC < 50%) and their length (RPKM). A SRC and a gene were associated with a minimum overlap of 20 nt. K-means clustering (iter.max=100) was used to define 3 groups of SRCs based on their RPKM coverage during wild-type autogamy time course experiments. siRNA transcription orientation ratio was calculated using counts obtained with SAMTools (samtools view). Unidirectional and bidirectional transcription ratios were calculated only for SRCs overlapping a gene and covered by at least 5 siRNA reads. mRNA RPKM coverage of SRCs was calculated using htseq-count (v0.11.2 stranded=no -mode=intersection-nonempty) on TopHat2 mappings (v2.1.1 --min-intron-length 15 --max-intron-length 100 --read-mismatch 1 --coverage-search) (Arnaiz et al., 2007).

DATA AVAILABILITY

sRNA-seq datasets generated for this study have been deposited at the ENA with Study Accession number PRJEB59349. The statistical data and R scripts used to generate the bioinformatic images, the original, unprocessed experimental data and numerical values were deposited at https://doi.org/10.5281/zenodo.8108886. All other relevant data supporting the key findings of this study are available within the article and its Supplemental Information files or from the corresponding author upon reasonable request.

FUNDING

This work was supported by the Centre National de la Recherche Scientifique, the Agence Nationale pour la Recherche (ANR) [project “LaMarque” ANR-18-CE12-0005 to SD] and [project “POLYCHROME” ANR-19-CE12-0015 to SD and OA]; the LABEX Who Am I? to SD (ANR-11-LABX-0071; ANR-11-IDEX-0005-02); the Fondation de la Recherche Médicale “Equipe FRM EQU202203014643” to SD. CMP was recipient of PhD fellowships from Université Paris Cité and Fondation ARC, and a LABEX Who Am I? transition postdoc fellowship, OC was recipient of PhD fellowships from Université Paris Cité and Fondation de la Recherche Médicale and of a EUR GENE transition postdoc fellowship.

ACKNOWLEDGEMENTS

We wish to thank the members of the Duharcourt lab for fruitful discussions. We thank Daniel Holoch and Eric Meyer for comments on the manuscript. We acknowledge the ImagoSeine facility, member of the FranceBioImaging infrastructure supported by the ANR-10-INSB-04, and the sequencing and bioinformatics expertise of the I2BC High-throughput sequencing facility, supported by France Génomique (funded by the French National Program "Investissement d’Avenir" ANR-10-INBS-09).

AUTHOR CONTRIBUTIONS

CMP conducted most experiments with the help of OC and AH for cloning and silencing experiments; AV with the help of MLA performed sRNA time course experiments; CMP and AF analyzed the Ezl1

catalytic mutant; OA designed and performed the bioinformatic analyses of NGS data; CMP, AV, SD designed the experiments and CMP, SD wrote the paper with input from all co-authors. SD supervised the project.

DECLARATION OF INTERESTS

The authors declare no competing interests.

REFERENCES

Allen, S.E., Hug, I., Pabian, S., Rzeszutek, I., Hoehener, C., Nowacki, M., 2017. Circular Concatemers of Ultra-Short DNA Segments Produce Regulatory RNAs. Cell 168, 990. https://doi.org/10.1016/j.cell.2017.02.020

Ardehali, M.B., Anselmo, A., Cochrane, J.C., Kundu, S., Sadreyev, R.I., Kingston, R.E., 2017. Polycomb Repressive Complex 2 Methylates Elongin A to Regulate Transcription. Mol. Cell 68, 872-884.e6. https://doi.org/10.1016/j.molcel.2017.10.025

Arnaiz, O., Cain, S., Cohen, J., Sperling, L., 2007. ParameciumDB: a community resource that integrates the Paramecium tetraurelia genome sequence with genetic data. Nucleic Acids Res. 35, D439-444. https://doi.org/10.1093/nar/gkl777

Arnaiz, O., Mathy, N., Baudry, C., Malinsky, S., Aury, J.-M., Denby Wilkes, C., Garnier, O., Labadie, K., Lauderdale, B.E., Le Mouël, A., Marmignon, A., Nowacki, M., Poulain, J., Prajer, M., Wincker, P., Meyer, E., Duharcourt, S., Duret, L., Bétermier, M., Sperling, L., 2012. The Paramecium Germline Genome Provides a Niche for Intragenic Parasitic DNA: Evolutionary Dynamics of Internal Eliminated Sequences. PLoS Genet. 8, e1002984. https://doi.org/10.1371/journal.pgen.1002984

Arnaiz, O., Meyer, E., Sperling, L., 2020. ParameciumDB 2019: integrating genomic data across the genus for functional and evolutionary biology. Nucleic Acids Res. 48, D599–D605. https://doi.org/10.1093/nar/gkz948

Aronica, L., Bednenko, J., Noto, T., DeSouza, L.V., Siu, K.W., Loidl, J., Pearlman, R.E., Gorovsky, M.A., Mochizuki, K., 2008. Study of an RNA helicase implicates small RNA-noncoding RNA interactions in programmed DNA elimination in Tetrahymena. Genes Dev 22, 2228–41.

Aury, J.M., Jaillon, O., Duret, L., Noel, B., Jubin, C., Porcel, B.M., Segurens, B., Daubin, V., Anthouard, V., Aiach, N., Arnaiz, O., Billaut, A., Beisson, J., Blanc, I., Bouhouche, K., Camara, F., Duharcourt, S., Guigo, R., Gogendeau, D., Katinka, M., Keller, A.M., Kissmehl, R., Klotz, C., Koll, F., Le Mouel, A., Lepere, G., Malinsky, S., Nowacki, M., Nowak, J.K., Plattner, H., Poulain, J., Ruiz, F., Serrano, V., Zagulski, M., Dessen, P., Betermier, M., Weissenbach, J., Scarpelli, C., Schachter, V., Sperling, L., Meyer, E., Cohen, J., Wincker, P., 2006. Global trends of whole-genome duplications revealed by the ciliate Paramecium tetraurelia. Nature 444, 171–8.

Baudry, C., Malinsky, S., Restituito, M., Kapusta, A., Rosa, S., Meyer, E., Betermier, M., 2009. PiggyMac, a domesticated piggyBac transposase involved in programmed genome rearrangements in the ciliate Paramecium tetraurelia. Genes Dev 23, 2478–83.

Beisson, J., Betermier, M., Bre, M.H., Cohen, J., Duharcourt, S., Duret, L., Kung, C., Malinsky, S., Meyer, E., Preer, J.R., Sperling, L., 2010a. Maintaining clonal Paramecium tetraurelia cell lines of controlled age through daily reisolation. Cold Spring Harb Protoc 2010, pdb prot5361.

Beisson, J., Betermier, M., Bre, M.H., Cohen, J., Duharcourt, S., Duret, L., Kung, C., Malinsky, S., Meyer, E., Preer, J.R., Sperling, L., 2010b. Mass culture of Paramecium tetraurelia. Cold Spring Harb Protoc 2010, pdb prot5362.

Bender, S., Tang, Y., Lindroth, A.M., Hovestadt, V., Jones, D.T.W., Kool, M., Zapatka, M., Northcott, P.A., Sturm, D., Wang, W., Radlwimmer, B., Højfeldt, J.W., Truffaux, N., Castel, D., Schubert, S., Ryzhova, M., Seker-Cin, H., Gronych, J., Johann, P.D., Stark, S., Meyer, J., Milde, T., Schuhmann, M., Ebinger, M., Monoranu, C.-M., Ponnuswami, A., Chen, S., Jones, C., Witt, O., Collins, V.P., von Deimling, A., Jabado, N., Puget, S., Grill, J., Helin, K., Korshunov, A., Lichter, P., Monje, M., Plass, C., Cho, Y.-J., Pfister, S.M., 2013. Reduced H3K27me3 and DNA hypomethylation are major drivers of gene expression in K27M mutant pediatric high-grade gliomas. Cancer Cell 24, 660–672. https://doi.org/10.1016/j.ccr.2013.10.006

Betermier, M., Duharcourt, S., 2014. Programmed Rearrangement in Ciliates: Paramecium. Microbiol. Spectr. 2. https://doi.org/10.1128/microbiolspec.MDNA3-0035-2014

Bouhouche, K., Gout, J.F., Kapusta, A., Betermier, M., Meyer, E., 2011. Functional specialization of Piwi proteins in Paramecium tetraurelia from post-transcriptional gene silencing to genome remodelling. Nucleic Acids Res 39, 4249–4264.

Brown, Z.Z., Müller, M.M., Jain, S.U., Allis, C.D., Lewis, P.W., Muir, T.W., 2014. Strategy for

"Detoxification" of a Cancer-Derived Histone Mutant Based on Mapping Its Interaction with the Methyltransferase PRC2. J. Am. Chem. Soc. 136, 13498–13501. https://doi.org/10.1021/ja5060934
Carradec, Q., Gotz, U., Arnaiz, O., Pouch, J., Simon, M., Meyer, E., Marker, S., 2015. Primary and secondary siRNA synthesis triggered by RNAs from food bacteria in the ciliate Paramecium tetraurelia. Nucleic Acids Res. 43, 1818–1833. https://doi.org/10.1093/nar/gku1331
de Vanssay, A., Touzeau, A., Arnaiz, O., Frapporti, A., Phipps, J., Duharcourt, S., 2020. The Paramecium histone chaperone Spt16-1 is required for Pgm endonuclease function in programmed genome rearrangements. PLoS Genet. 16, e1008949. https://doi.org/10.1371/journal.pgen.1008949
Duharcourt, S., Butler, A., Meyer, E., 1995. Epigenetic self-regulation of developmental excision of an internal eliminated sequence on Paramecium tetraurelia. Genes Dev 9, 2065–77.
Duharcourt, S., Keller, A.M., Meyer, E., 1998. Homology-dependent maternal inhibition of developmental excision of internal eliminated sequences in Paramecium tetraurelia. Mol Cell Biol 18, 7075–85.
Frapporti, A., Miró Pina, C., Arnaiz, O., Holoch, D., Kawaguchi, T., Humbert, A., Eleftheriou, E., Lombard, B., Loew, D., Sperling, L., Guitot, K., Margueron, R., Duharcourt, S., 2019. The Polycomb protein Ezl1 mediates H3K9 and H3K27 methylation to repress transposable elements in Paramecium. Nat. Commun. 10, 2710. https://doi.org/10.1038/s41467-019-10648-5
Furrer, D.I., Swart, E.C., Kraft, M.F., Sandoval, P.Y., Nowacki, M., 2017. Two Sets of Piwi Proteins Are Involved in Distinct sRNA Pathways Leading to Elimination of Germline-Specific DNA. Cell Rep. 20, 505–520. https://doi.org/10.1016/j.celrep.2017.06.050
Gruchota, J., Denby Wilkes, C., Arnaiz, O., Sperling, L., Nowak, J.K., 2017. A meiosis-specific Spt5 homolog involved in non-coding transcription. Nucleic Acids Res. gkw1318. https://doi.org/10.1093/nar/gkw1318
Guérin, F., Arnaiz, O., Boggetto, N., Denby Wilkes, C., Meyer, E., Sperling, L., Duharcourt, S., 2017. Flow cytometry sorting of nuclei enables the first global characterization of Paramecium germline DNA and transposable elements. BMC Genomics 18, 327. https://doi.org/10.1186/s12864-017-3713-7
Han, J., LaVigne, C.A., Jones, B.T., Zhang, H., Gillett, F., Mendell, J.T., 2020. A ubiquitin ligase mediates target-directed microRNA decay independently of tailing and trimming. Science 370, eabc9546. https://doi.org/10.1126/science.abc9546
Han, J., Mendell, J.T., 2023. MicroRNA turnover: a tale of tailing, trimming, and targets. Trends Biochem. Sci. 48, 26–39. https://doi.org/10.1016/j.tibs.2022.06.005
He, A., Shen, X., Ma, Q., Cao, J., von Gise, A., Zhou, P., Wang, G., Marquez, V.E., Orkin, S.H., Pu, W.T., 2012. PRC2 directly methylates GATA4 and represses its transcriptional activity. Genes Dev. 26, 37–42. https://doi.org/10.1101/gad.173930.111
Ignarski, M., Singh, A., Swart, E.C., Arambasic, M., Sandoval, P.Y., Nowacki, M., 2014. Paramecium tetraurelia chromatin assembly factor-1-like protein PtCAF-1 is involved in RNA-mediated control of DNA elimination. Nucleic Acids Res. 42, 11952–11964. https://doi.org/10.1093/nar/gku874
Jain, S.U., Rashoff, A.Q., Krabbenhoft, S.D., Hoelper, D., Do, T.J., Gibson, T.J., Lundgren, S.M., Bondra, E.R., Deshmukh, S., Harutyunyan, A.S., Juretic, N., Jabado, N., Harrison, M.M., Lewis, P.W., 2020. H3 K27M and EZHIP Impede H3K27-Methylation Spreading by Inhibiting Allosterically Stimulated PRC2. Mol. Cell 80, 726-735.e7. https://doi.org/10.1016/j.molcel.2020.09.028
Ji, L., Chen, X., 2012. Regulation of small RNA stability: methylation and beyond. Cell Res. 22, 624–636. https://doi.org/10.1038/cr.2012.36
Johnson, N.R., Yeoh, J.M., Coruh, C., Axtell, M.J., 2016. Improved Placement of Multi-mapping Small RNAs. G3 Bethesda Md 6, 2103–2111. https://doi.org/10.1534/g3.116.030452
Karunanithi, S., Oruganti, V., Marker, S., Rodriguez-Viana, A.M., Drews, F., Pirritano, M., Nordström, K., Simon, M., Schulz, M.H., 2019. Exogenous RNAi mechanisms contribute to transcriptome adaptation by phased siRNA clusters in Paramecium. Nucleic Acids Res. 47, 8036–8049. https://doi.org/10.1093/nar/gkz553
Kurth, H.M., Mochizuki, K., 2009. 2'-O-methylation stabilizes Piwi-associated small RNAs and ensures DNA elimination in Tetrahymena. Rna 15, 675–85.

Lee, J.M., Lee, J.S., Kim, H., Kim, K., Park, H., Kim, J.-Y., Lee, S.H., Kim, I.S., Kim, J., Lee, M., Chung, C.H., Seo, S.-B., Yoon, J.-B., Ko, E., Noh, D.-Y., Kim, K.I., Kim, K.K., Baek, S.H., 2012. EZH2 generates a methyl degron that is recognized by the DCAF1/DDB1/CUL4 E3 ubiquitin ligase complex. Mol. Cell 48, 572–586. https://doi.org/10.1016/j.molcel.2012.09.004
Lepere, G., Betermier, M., Meyer, E., Duharcourt, S., 2008. Maternal noncoding transcripts antagonize the targeting of DNA elimination by scanRNAs in Paramecium tetraurelia. Genes Dev 22, 1501–12.
Lepere, G., Nowacki, M., Serrano, V., Gout, J.F., Guglielmi, G., Duharcourt, S., Meyer, E., 2009. Silencing-associated and meiosis-specific small RNA pathways in Paramecium tetraurelia. Nucleic Acids Res 37, 903–15.
Lewis, P.W., Müller, M.M., Koletsky, M.S., Cordero, F., Lin, S., Banaszynski, L.A., Garcia, B.A., Muir, T.W., Becher, O.J., Allis, C.D., 2013. Inhibition of PRC2 Activity by a Gain-of-Function H3 Mutation Found in Pediatric Glioblastoma. Science 340, 857–861. https://doi.org/10.1126/science.1232245
Lhuillier-Akakpo, M., Frapporti, A., Denby Wilkes, C., Matelot, M., Vervoort, M., Sperling, L., Duharcourt, S., 2014. Local effect of enhancer of zeste-like reveals cooperation of epigenetic and cis-acting determinants for zygotic genome rearrangements. PLoS Genet. 10, e1004665. https://doi.org/10.1371/journal.pgen.1004665
Lhuillier-Akakpo, M., Guérin, F., Frapporti, A., Duharcourt, S., 2016. DNA deletion as a mechanism for developmentally programmed centromere loss. Nucleic Acids Res. 44, 1553–1565. https://doi.org/10.1093/nar/gkv1110
Maliszewska-Olejniczak, K., Gruchota, J., Gromadka, R., Denby Wilkes, C., Arnaiz, O., Mathy, N., Duharcourt, S., Bétermier, M., Nowak, J.K., 2015. TFIIS-Dependent Non-coding Transcription Regulates Developmental Genome Rearrangements. PLoS Genet. 11, e1005383. https://doi.org/10.1371/journal.pgen.1005383
Margueron, R., Li, G., Sarma, K., Blais, A., Zavadil, J., Woodcock, C.L., Dynlacht, B.D., Reinberg, D., 2008. Ezh1 and Ezh2 maintain repressive chromatin through different mechanisms. Mol. Cell 32, 503–518. https://doi.org/10.1016/j.molcel.2008.11.004
Marker, S., Carradec, Q., Tanty, V., Arnaiz, O., Meyer, E., 2014. A forward genetic screen reveals essential and non-essential RNAi factors in Paramecium tetraurelia. Nucleic Acids Res. 42, 7268–7280. https://doi.org/10.1093/nar/gku223
Marker, S., Le Mouel, A., Meyer, E., Simon, M., 2010. Distinct RNA-dependent RNA polymerases are required for RNAi triggered by double-stranded RNA versus truncated transgenes in Paramecium tetraurelia. Nucleic Acids Res. 38, 4092–4107. https://doi.org/10.1093/nar/gkq131
Martienssen, R., Moazed, D., 2015. RNAi and Heterochromatin Assembly. Cold Spring Harb. Perspect. Biol. 7, a019323. https://doi.org/10.1101/cshperspect.a019323
Martinez, N.J., Gregory, R.I., 2013. Argonaute2 expression is post-transcriptionally coupled to microRNA abundance. RNA 19, 605–612. https://doi.org/10.1261/rna.036434.112
Miró-Pina, C., Charmant, O., Kawaguchi, T., Holoch, D., Michaud, A., Cohen, I., Humbert, A., Jaszczyszyn, Y., Chevreux, G., Maestro, L.D., Ait-Si-Ali, S., Arnaiz, O., Margueron, R., Duharcourt, S., 2022. Paramecium Polycomb repressive complex 2 physically interacts with the small RNA-binding PIWI protein to repress transposable elements. Dev. Cell 57, 1037-1052.e8. https://doi.org/10.1016/j.devcel.2022.03.014
Mochizuki, K., Fine, N.A., Fujisawa, T., Gorovsky, M.A., 2002. Analysis of a piwi-related gene implicates small RNAs in genome rearrangement in tetrahymena. Cell 110, 689–99.
Owsian, D., Gruchota, J., Arnaiz, O., Nowak, J.K., 2022. The transient Spt4-Spt5 complex as an upstream regulator of non-coding RNAs during development. Nucleic Acids Res. gkac106. https://doi.org/10.1093/nar/gkac106
Sandoval, P.Y., Swart, E.C., Arambasic, M., Nowacki, M., 2014. Functional Diversification of Dicer-like Proteins and Small RNAs Required for Genome Sculpting. Dev. Cell 28, 174–188. https://doi.org/10.1016/j.devcel.2013.12.010
Sanulli, S., Justin, N., Teissandier, A., Ancelin, K., Portoso, M., Caron, M., Michaud, A., Lombard, B., da Rocha, S.T., Offer, J., Loew, D., Servant, N., Wassef, M., Burlina, F., Gamblin, S.J., Heard, E.,

Margueron, R., 2015. Jarid2 Methylation via the PRC2 Complex Regulates H3K27me3 Deposition during Cell Differentiation. Mol. Cell 57, 769–783. https://doi.org/10.1016/j.molcel.2014.12.020
Sarthy, J.F., Meers, M.P., Janssens, D.H., Henikoff, J.G., Feldman, H., Paddison, P.J., Lockwood, C.M., Vitanza, N.A., Olson, J.M., Ahmad, K., Henikoff, S., 2020. Histone deposition pathways determine the chromatin landscapes of H3.1 and H3.3 K27M oncohistones. eLife 9, e61090. https://doi.org/10.7554/eLife.61090
Schoeberl, U.E., Kurth, H.M., Noto, T., Mochizuki, K., 2012. Biased transcription and selective degradation of small RNAs shape the pattern of DNA elimination in Tetrahymena. Genes Dev. 26, 1729–1742. https://doi.org/10.1101/gad.196493.112
Sellis, D., Guérin, F., Arnaiz, O., Pett, W., Lerat, E., Boggetto, N., Krenek, S., Berendonk, T., Couloux, A., Aury, J.-M., Labadie, K., Malinsky, S., Bhullar, S., Meyer, E., Sperling, L., Duret, L., Duharcourt, S., 2021. Massive colonization of protein-coding exons by selfish genetic elements in Paramecium germline genomes. PLOS Biol. 19, e3001309. https://doi.org/10.1371/journal.pbio.3001309
Shi, C.Y., Kingston, E.R., Kleaveland, B., Lin, D.H., Stubna, M.W., Bartel, D.P., 2020. The ZSWIM8 ubiquitin ligase mediates target-directed microRNA degradation. Science 370, eabc9359. https://doi.org/10.1126/science.abc9359
Singh, D.P., Saudemont, B., Guglielmi, G., Arnaiz, O., Goût, J.-F., Prajer, M., Potekhin, A., Przybòs, E., Aubusson-Fleury, A., Bhullar, S., Bouhouche, K., Lhuillier-Akakpo, M., Tanty, V., Blugeon, C., Alberti, A., Labadie, K., Aury, J.-M., Sperling, L., Duharcourt, S., Meyer, E., 2014. Genome-defence small RNAs exapted for epigenetic mating-type inheritance. Nature 509, 447–452. https://doi.org/10.1038/nature13318
Smibert, P., Yang, J.-S., Azzam, G., Liu, J.-L., Lai, E.C., 2013. Homeostatic control of Argonaute stability by microRNA availability. Nat. Struct. Mol. Biol. 20, 789–795. https://doi.org/10.1038/nsmb.2606
Solberg, T., Mason, V., Wang, C., Nowacki, M., 2023. Developmental mRNA clearance by PIWI-bound endo-siRNAs in Paramecium. Cell Rep. 42, 112213. https://doi.org/10.1016/j.celrep.2023.112213
Stafford, J.M., Lee, C.-H., Voigt, P., Descostes, N., Saldaña-Meyer, R., Yu, J.-R., Leroy, G., Oksuz, O., Chapman, J.R., Suarez, F., Modrek, A.S., Bayin, N.S., Placantonakis, D.G., Karajannis, M.A., Snuderl, M., Ueberheide, B., Reinberg, D., 2018. Multiple modes of PRC2 inhibition elicit global chromatin alterations in H3K27M pediatric glioma. Sci. Adv. 4, eaau5935. https://doi.org/10.1126/sciadv.aau5935
Wang, C., Solberg, T., Maurer-Alcalá, X.X., Swart, E.C., Gao, F., Nowacki, M., 2022. A small RNA-guided PRC2 complex eliminates DNA as an extreme form of transposon silencing. Cell Rep. 40. https://doi.org/10.1016/j.celrep.2022.111263
Zangarelli, C., Arnaiz, O., Bourge, M., Gorrichon, K., Jaszczyszyn, Y., Mathy, N., Escoriza, L., Betermier, M., Regnier, V., 2022. Developmental timing of programmed DNA elimination in Paramecium tetraurelia recapitulates germline transposon evolutionary dynamics. Genome Res. gr.277027.122. https://doi.org/10.1101/gr.277027.122
Zhang, Q., Agius, S.C., Flanigan, S.F., Uckelmann, M., Levina, V., Owen, B.M., Davidovich, C., 2021. PALI1 facilitates DNA and nucleosome binding by PRC2 and triggers an allosteric activation of catalysis. Nat. Commun. 12, 4592. https://doi.org/10.1038/s41467-021-24866-3

Figure legends

Figure 1. sRNA dynamics during *Paramecium* sexual cycle.
A. The genome scanning model. The progression of nuclear developmental events during autogamy is represented above, and below, the molecular steps of the scanning model. (i) scnRNA biogenesis. During meiosis, 25-nt scnRNA are produced by the Dicer-like proteins Dcl2/3 from the whole MIC genome (MAC-destined sequences in black, MIC-specific sequences in orange) and are loaded onto Ptiwi01/09. (ii) scnRNA selection. Ptiwi–scnRNA complexes are transported to the maternal MAC. Homologous pairing between scnRNAs and MAC non-coding RNAs (ncRNA) leads to the degradation of MAC-scnRNAs (black) and selection of MIC-specific scnRNAs (orange) that are then transported to the new developing MAC. (iii) scnRNA-guided histone mark deposition and DNA elimination. scnRNAs are thought to recognize homologous sequences by base-pairing interactions with nascent ncRNAs in the new developing MACs. Interaction between Ptiwi09 and the PRC2 complex guides the deposition of H3K9me3 and H3K27me3 on MIC-specific sequences. These histone marks would guide the recruitment of the excision complex, allowing elimination of MIC-specific sequences (orange).
B. Analysis of small RNA populations in vegetative cells and at different times of the sexual cycle (see Figure S1 for the description of the time points).
C. Representative genomic region depicting 25-nt scnRNAs at different time points of the sexual cycle.
D. Percentage of the genome covered by 25-nt scnRNAs.

Figure 2. Developmental-specific 23-nt short-read clusters.
A. Heatmap of the 136 short-read clusters (SRCs) showing the normalized 23-nt sRNA coverage (log RPKM) during autogamy time course experiments. Based on their coverage, SRCs were split in 3 groups by K-means hierarchical clustering on the heatmap. The first group, induced during autogamy (from T=5 hours), contains 29 SRCs (SRC001 to SRC029). The second and third groups contain 64 and 43 SRCs, respectively, that are constitutively expressed at different levels (lowly for the 2nd and highly for the 3rd).
B. Heatmap showing the 23-nt sRNA transcription orientation for the 29 developmental-specific SRCs (first group in (A)). White indicates a 50% bidirectional transcription ratio and green a unidirectional transcription ratio. The 16 SRCs which overlap a putative coding gene are in bold. The only SRC that is transcribed in the same orientation than its overlapping gene is in red.
C. Heatmap showing the normalized mRNA coverage (log RPKM) for the developmental-specific SRCs.
D. Circos representation of the 29 developmental-specific SRCs (black circles). The blue circles represent the part of SRC covered by a predicted gene. Histograms represent the sequencing coverage at T=10 and at T=20 hours: mRNA coverage (blue), and 23-nt sRNA coverage in wild-type condition (green), rdr1 mutant (purple) and rdr2 mutant (orange). The blue arcs represent paralogous links from the most recent WGD between SRCs.
E. Boxplot showing global 23-nt sRNA coverage for developmental-specific SRCs at 3 time points (T=0, T=10 and T=20 hours) in 3 conditions: wild-type, rdr1 mutant and rdr2 mutant.

Figure 3. PRC2-Ezl1 core complex and its associated cofactors are involved in scnRNA selection.
A. Left: Normalized counts of 25nt-long scnRNAs at T=0 hours in control (CTL), *EZL1, SUZ12.like, RF2, EAP1, RF4* and *DCL2/3* RNAi conditions. Bar plots show the reads that are unmapped or match the MAC genome, IESs and OES reference sequences. Right: Proportion of 25nt-long scnRNAs that match the MAC genome, IESs and OES reference sequences at different time points of the sexual cycle in control (CTL), *EZL1, SUZ12.like, RF2, EAP1,* and *RF4* RNAi conditions.
B. Representative genomic region depicting 25-nt scnRNAs at T=35 hours in control (CTL), *EZL1, SUZ12.like, RF2, EAP1,* and *RF4* RNAi
C. GFP-Ptiwi09 localization in CTL, *DCL2/3* and *EZL1* RNAi conditions in meiosis and during MAC development. Representative images are displayed. Overlay of Z-projections are presented. Dashed white circles indicate the new developing MACs. Scale bar is 10 µm.

Figure 4. Ezl1 catalytic activity is not required for scnRNA selection.

A. H3K27me3 immunostaining of non-injected cells (NI), and of cells transformed with *H3P1*^{K27M} or *H3P3*^{K27M} during MAC development. Representative images are displayed. Overlay of Z-projections are presented. Dashed white circles indicate the new developing MACs. Scale bar is 10 µm.

B. Production of sexual progeny in cells transformed with *H3P1*^{K27M} or *H3P3*^{K27M}. The total number of analyzed cells and the number of independent experiments (in parenthesis) are indicated.

C. Left: Normalized counts of 25-nt scnRNAs at T=0 hours in control (CTL) RNAi conditions, in cells transformed with *GFP-EZL1*^{H526A} upon endogenous *EZL1* RNAi and in cells transformed with *H3P1*^{K27M}. Bar plots show the reads that are unmapped or match the MAC genome, IESs and OES reference sequences. Right: Proportion of 25-nt scnRNAs that match the MAC genome, IESs and OES reference sequences at T=0 and T=20 hours of the sexual cycle.

D. H3K27me3 immunostaining and *GFP-EZL1*^{H526A} localization during new MAC development in cells transformed with *GFP-EZL1*^{H526A} upon endogenous *EZL1* RNAi. Representative images are displayed. Overlay of Z-projections of magnified views of Hoechst staining, H3K27me3-specific antibody and GFP signal are presented. Dashed white circles indicate the new developing MACs. Scale bar is 10 µm.

E. Model for scnRNA selection. The presence of PRC2 core subunits and cofactors in the maternal MAC but not the deposition of H3K27me3 appears to be required for the degradation of MAC-scnRNAs.

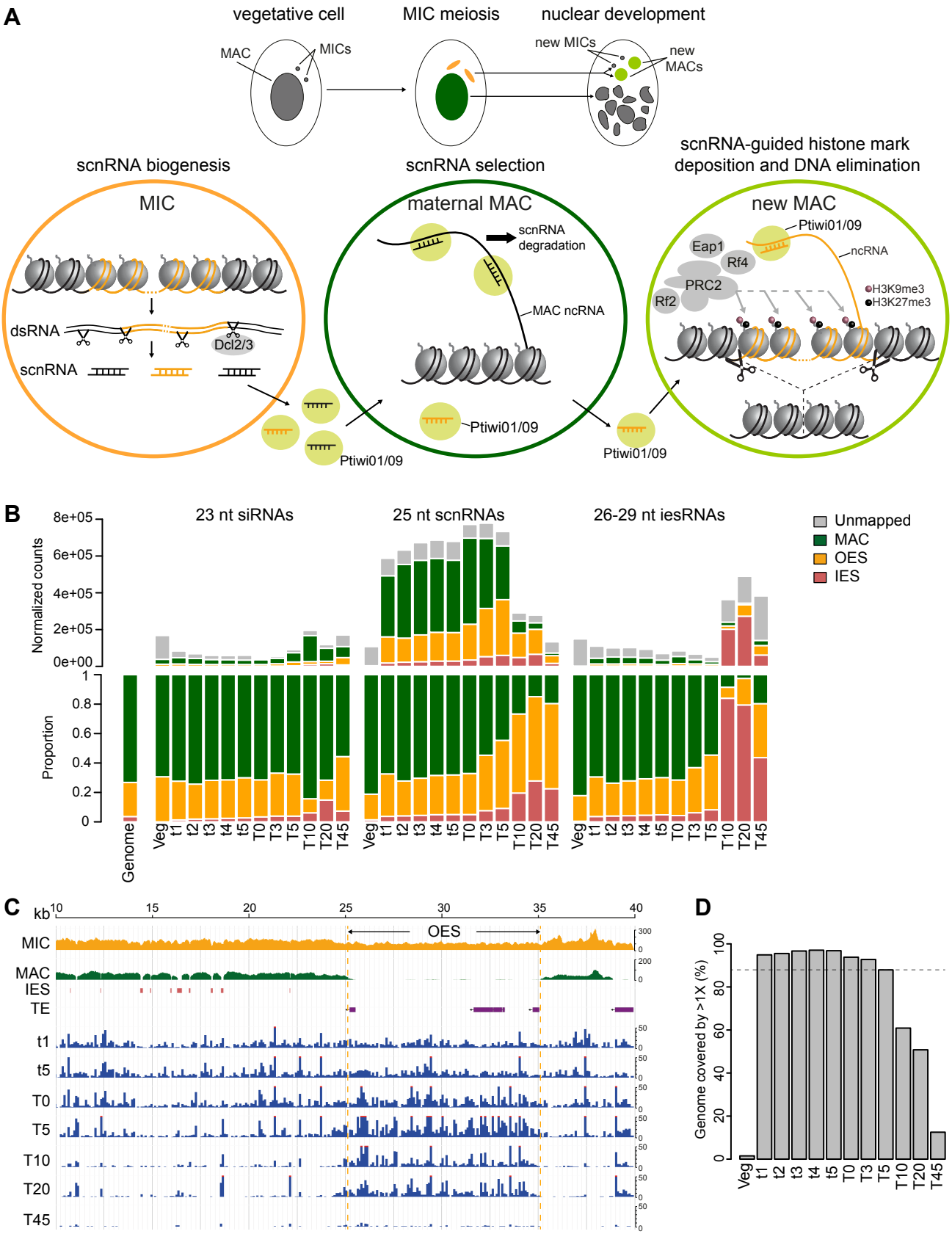

Figure 1. sRNA dynamics during *Paramecium* sexual cycle.

A. The genome scanning model. The progression of nuclear developmental events during autogamy is represented above, and below, the molecular steps of the scanning model. (i) scnRNA biogenesis. During meiosis, 25-nt scnRNA are produced by the Dicer-like proteins Dcl2/3 from the whole MIC genome (MAC-destined sequences in black, MIC-specific sequences in orange) and are loaded onto Ptiwi01/09. (ii) scnRNA selection. Ptiwi–scnRNA complexes are transported to the maternal MAC. Homologous pairing between scnRNAs and MAC non-coding RNAs (ncRNA) leads to the degradation of MAC-scnRNAs (black) and selection of MIC-specific scnRNAs (orange) that are then transported to the new developing MAC. (iii) scnRNA-guided histone mark deposition and DNA elimination. scnRNAs are thought to recognize homologous sequences by base-pairing interactions with nascent ncRNAs in the new developing MACs. Interaction between Ptiwi09 and the PRC2 complex guides the deposition of H3K9me3 and H3K27me3 on MIC-specific sequences. These histone marks would guide the recruitment of the excision complex, allowing elimination of MIC-specific sequences (orange).

B. Analysis of small RNA populations in vegetative cells and at different times of the sexual cycle (see Figure S1 for the description of the time points).

C. Representative genomic region depicting 25-nt scnRNAs at different time points of the sexual cycle.

D. Percentage of the genome covered by 25-nt scnRNAs.

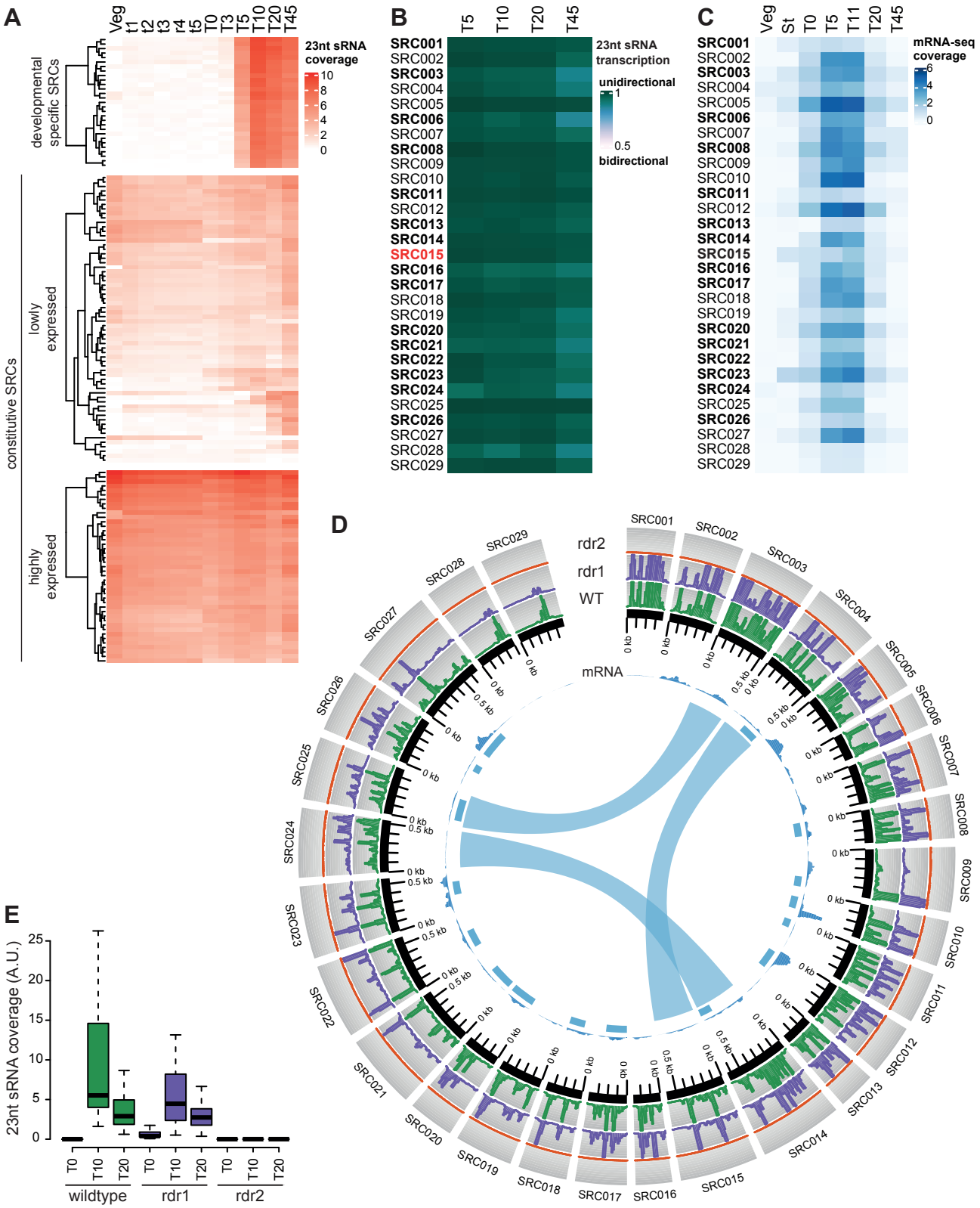

Figure 2. Developmental-specific 23 nt short-read clusters.

A. Heatmap of the 136 short-read clusters (SRC) showing the normalized 23-nt sRNA coverage (log RPKM) during autogamy time course experiments. Based on their coverage, SRCs were split in 3 groups by K-means hierarchical clustering on the heatmap. The first group, induced during autogamy (from T=5), contains 29 SRCs (SRC001 to SRC029). The second and third groups contain 64 and 43 SRCs respectively, that are constitutively expressed at different levels (lowly for the second and highly for the third).

B. Heatmap showing the 23-nt sRNA transcription orientation for the 29 developmental-specific SRCs (first group in (A)). White indicates a 50% bidirectional transcription ratio and green a unidirectional transcription ratio. The 16 SRCs which overlap a putative coding gene are in bold. The only SRC that is transcribed in the same orientation than its overlapping gene is in red.

C. Heatmap showing the normalized mRNA coverage (log RPKM) for the developmental-specific SRCs.

D. Circos representation of the 29 developmental-specific SRCs (black circles). The blue circles represent the part of SRC covered by a predicted gene. Histograms represent the sequencing coverage at T=10 and at T=20 hours: mRNA coverage (blue), and 23-nt sRNA coverage in wild-type condition (green), rdr1 mutant (purple) and rdr2 mutant (orange). The blue arcs represent paralogous links from the most recent WGD between SRCs.

E. Boxplot showing global 23-nt sRNA coverage for developmental-specific SRCs at 3 time points (T=0, T=10 and T=20 hours) in 3 conditions: wild-type, rdr1 mutant and rdr2 mutant.

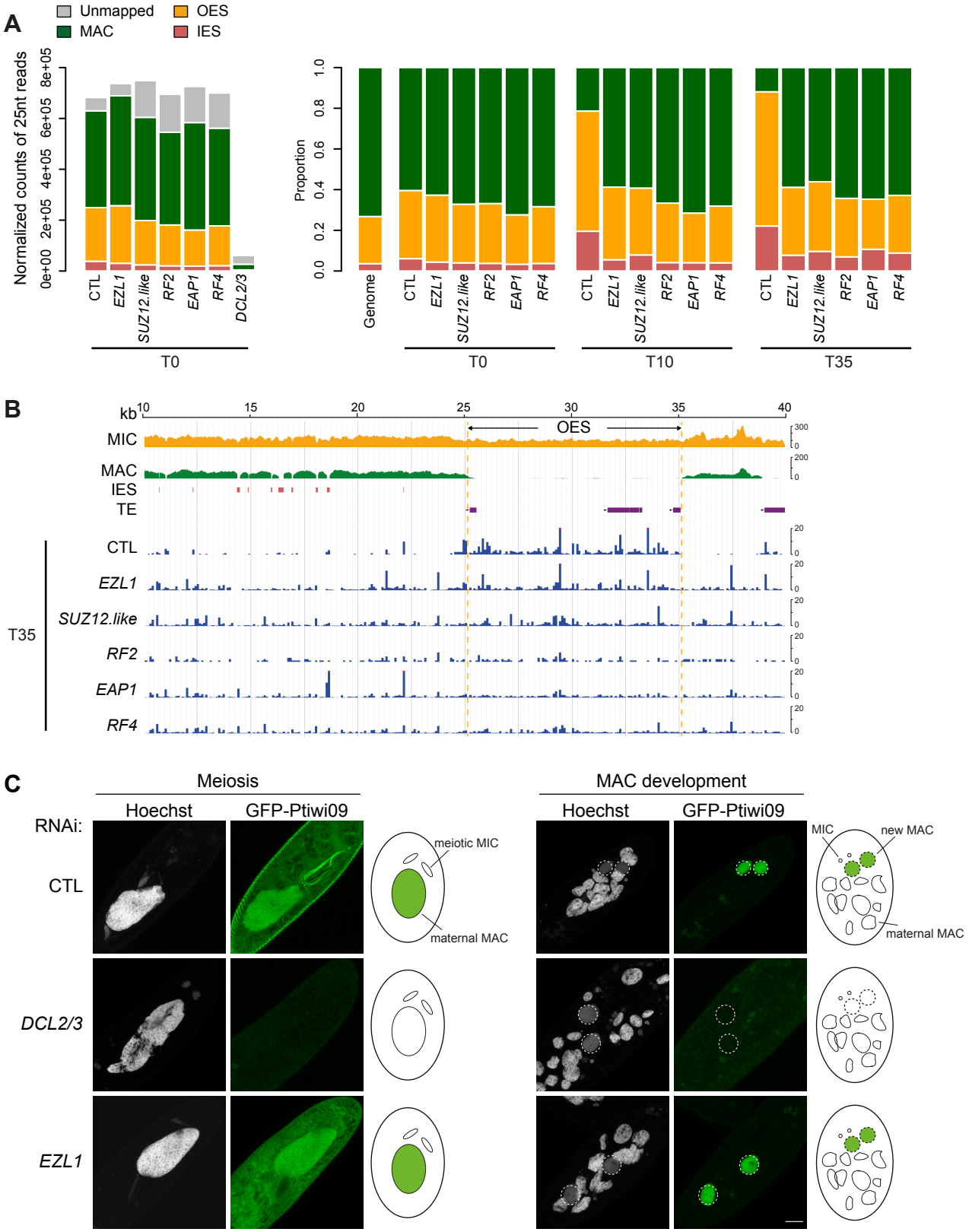

Figure 3. PRC2-Ezl1 core complex and its associated cofactors are involved in scnRNA selection.

A. Left: Normalized counts of 25nt-long scnRNAs at T=0 hours in control (CTL), *EZL1, SUZ12.like*, *RF2, EAP1, RF4* and *DCL2/3* RNAi conditions. Bar plots show the reads that are unmapped or match the MAC genome, IESs and OES reference sequences. Right: Proportion of 25nt-long scnRNAs that match the MAC genome, IESs and OES reference sequences at different times of the sexual cycle in control (CTL), *EZL1, SUZ12.like*, *RF2, EAP1,* and *RF4* RNAi conditions.

B. Representative genomic region depicting 25-nt scnRNAs at T=35 in control (CTL), *EZL1, SUZ12.like*, *RF2, EAP1,* and *RF4* RNAi.

C. GFP-Ptiwi09 localization in CTL, *DCL2/3* and *EZL1* RNAi conditions in meiosis and during MAC development. Representative images are displayed. Overlay of Z-projections are presented. Dashed white circles indicate the new developing MACs. Scale bar is 10 µm.

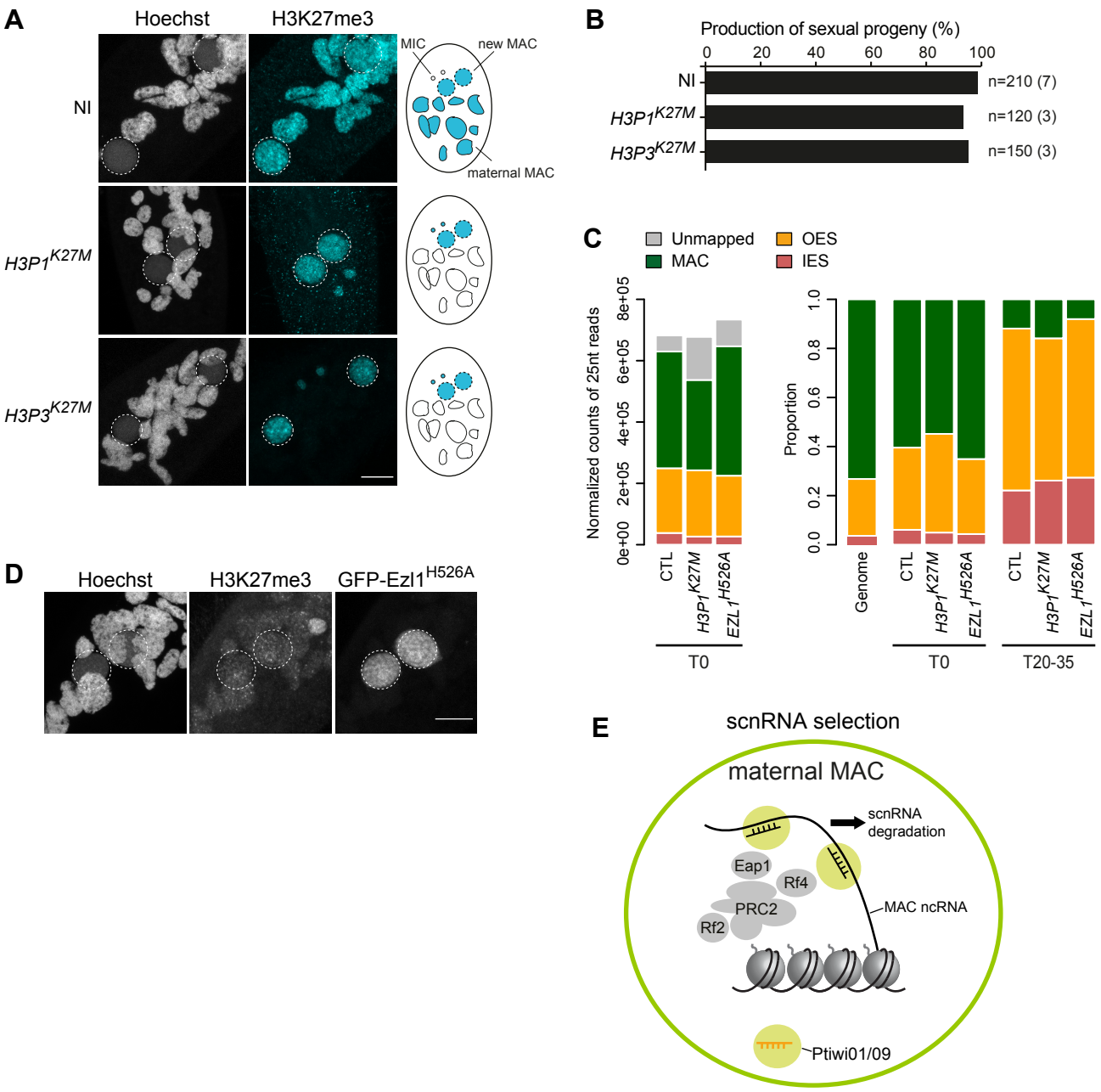

Figure 4. Ezl1 catalytic activity is not required for scnRNA selection.

A. H3K27me3 immunostaining of non-injected cells (NI), and of cells transformed with *H3P1*^{K27M} or *H3P3*^{K27M} during MAC development. Representative images are displayed. Overlay of Z-projections are presented. Dashed white circles indicate the new developing MACs. Scale bar is 10 µm.

B. Production of sexual progeny in cells transformed with *H3P1*^{K27M} or *H3P3*^{K27M}. The total number of analyzed cells and the number of independent experiments (in parenthesis) are indicated.

C. Left: Normalized counts of 25-nt scnRNAs at T=0 hours in control (CTL) RNAi conditions, in cells transformed with *GFP-EZL1*^{H526A} upon endogenous *EZL1* RNAi and in cells transformed with *H3P1*^{K27M}. Bar plots show the reads that are unmapped or match the MAC genome, IESs and OES reference sequences. Right: Proportion of 25-nt scnRNAs that match the MAC genome, IESs and OES reference sequences at T=0 and T=20 hours of the sexual cycle.

D. H3K27me3 immunostaining and GFP-Ezl1^{H526A} localization during MAC development in cells transformed with *GFP-EZL1*^{H526A} transgene upon endogenous *EZL1* RNAi. Representative images are displayed. Overlay of Z-projections of magnified views of Hoechst staining, H3K27me3-specific antibody and GFP signal are presented. Dashed white circles indicate the new MACs. Scale bar is 10 µm.

E. Model for the scnRNA selection process. The presence of PRC2 core subunits and cofactors in the maternal MAC, but not the deposition of H3K27me3, appears to be required for the MAC-scnRNA degradation.